

# The quasi-periodic Bose-Hubbard model and localization in one-dimensional cold atomic gases

G. Roux,<sup>1,\*</sup> T. Barthel,<sup>1</sup> I. P. McCulloch,<sup>2</sup> C. Kollath,<sup>3</sup> U. Schollwöck,<sup>1</sup> and T. Giamarchi<sup>4</sup>

<sup>1</sup>*Institute for Theoretical Physics C, RWTH Aachen, D-52056 Aachen, Germany*

<sup>2</sup>*School of Physical Sciences, The University of Queensland, Brisbane, QLD, 4072, Australia*

<sup>3</sup>*Centre de Physique Théorique, Ecole Polytechnique, 91128 Palaiseau Cedex, France*

<sup>4</sup>*DPMC-MaNEP, University of Geneva, 24 Quai Ernest-Ansermet, CH-1211 Geneva, Switzerland*

(Dated: October 16, 2021)

We compute the phase diagram of the one-dimensional Bose-Hubbard model with a quasi-periodic potential by means of the density-matrix renormalization group technique. This model describes the physics of cold atoms loaded in an optical lattice in the presence of a superlattice potential whose wave length is incommensurate with the main lattice wave length. After discussing the conditions under which the model can be realized experimentally, the study of the density vs. the chemical potential curves for a non-trapped system uncovers the existence of gapped phases for incommensurate densities interpreted as incommensurate charge-density wave phases. Furthermore, a localization transition is known to occur above a critical value of the potential depth  $V_2$  in the case of free and hard-core bosons. We extend these results to soft-core bosons for which the phase diagrams at fixed density display new features compared with the phase diagram known for a random box distribution disorder. In particular, a direct transition from the superfluid phase to the Mott insulating phase is found at finite  $V_2$ . Evidences for reentrances of the superfluid phase upon increasing interactions are presented. We finally comment on different ways to probe the occurring quantum phases and most importantly the existence of a critical value for the localization transition. The latter feature can be investigated by looking at the expansion of the cloud after releasing the trap.

PACS numbers:

Disordered media are known to allow for the localization of waves in many physical systems both quantum and classical. As demonstrated by Anderson [1, 2], increasing disorder induces a transition to an insulating state. The occurrence of this Anderson transition strongly depends on the dimensionality of the system: in one-dimension a localized phase is expected as soon as disorder is present [3]. One of the key question in the field of strongly correlated systems is the interplay between interactions and disorder. Using field theoretical methods [4, 5], it was shown for one dimensional systems of bosons and fermions that interactions can lead to a localization-delocalization transition. For one dimensional [4, 5] or higher dimensional [6] bosons, the combination of interactions and disorder leads to a transition between a superfluid phase for weakly repulsive bosons and a localized phase (Bose glass) for strong repulsion. When an additional commensurate potential is present, there is a competition between the possible three phases, namely the superfluid (SF) phase, the Mott insulating (MI) phase which occurs for commensurate fillings and large interactions, and the so-called Bose-glass (BG) phase which is induced by disorder. Numerical confirmations [7, 8] came to support the general picture and to provide phase diagrams [9, 10] in one dimension where mean-field theory fails. However, experimental set-ups in solid state physics lack a good control of the interactions and the amount of disorder. More recently, cold atomic gases offered the possibility of a fine-tuning of the hamiltonian parameters in particularly clean set-ups. As a paradigm for strongly interacting gases, the SF-MI phase transition was demonstrated using an optical lattice [11]. A

fine-tuning is as well conceivable for the disorder strength. In this direction, several proposals were put forward: the use of a laser speckle [12, 13, 14, 15, 16, 17], the use of heavy atoms which provide a quasi-static potential for lighter atoms [18, 19], and finally the addition of a superlattice potential with a wave length which is incommensurate with the lattice potential wave length [20, 21, 22, 23].

This paper is devoted to the study of the latter situation, the so-called bichromatic set-up, for which experiments have recently been carried out [22, 23]. The one-particle Schrödinger equation with an incommensurate lattice has been widely studied [21, 24, 25, 26, 27, 28, 29, 30] and was found to exhibit anomalous diffusion properties [31, 32]. The main result of these studies, as we will recall later on, is the existence of a critical value of the potential above which localization occurs. For the many-body physics, a weak-coupling treatment of the potential was carried out using bosonisation [33, 34]. Quasiperiodic potentials were found to have an intermediate behavior between commensurate ones, and disordered ones. Exact numerical results on the Bose-Hubbard model with a quasi-periodic potential already exist [35, 36, 37] but are limited to small systems and thus cannot investigate the nature of the transition nor their precise location. The physics of the Bose-Hubbard model with a *periodic* superlattice has been investigated [38, 39, 40] and a “weakly superfluid” phase at large potential depth was found [38]. Very recently, Roscilde [41] carried out a more detailed study using quantum Monte Carlo calculations and a “random atomic limit” approach. He gives an accurate description of the trapped gas and of static observables. However, he did not describe the phase diagrams at fixed density.

Our main motivation is to address the shape of these fixed-density phase diagrams for a one-dimensional system using the density-matrix renormalization group (DMRG) algorithm

---

\*Electronic address: roux@physik.rwth-aachen.de

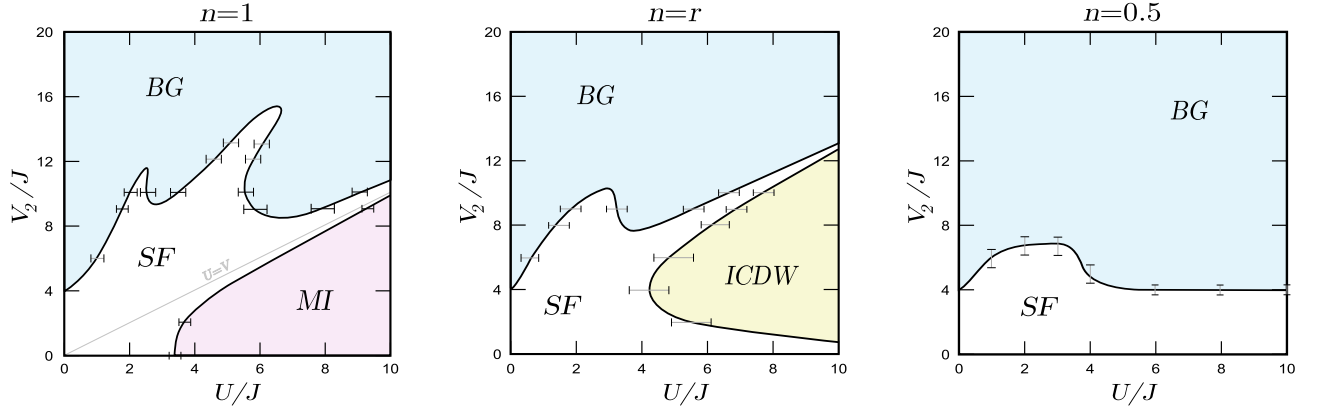


FIG. 1: (Color online) *Phase diagrams of the bichromatic Bose-Hubbard model for densities  $n = 1$ ,  $r$  (the ratio of the potential wave lengths) and  $n = 0.5$ .* The diagrams are shown as a function of the interaction strength  $U$  and the incommensurate potential strength  $V_2$ , both normalized by the hopping  $J$  (lines are guides to the eyes). *SF* stands for the superfluid phase, *MI* for the Mott-insulating phase, *BG* for the “Bose-glass” phase (meaning localized but with zero one-particle gap) and *ICDW* for incommensurate charge-density wave phase. The  $U = V_2$  line on the phase diagram with  $n = 1$  indicates the  $J = 0$  limit for which the gap of the one-particle excitation vanishes. Black error bars are deduced from calculations with averaging over the phase-shift  $\phi$  (cf. Sec. IA) and finite-size scaling (see Figs. 12 and 13 for details on the  $n = 1$  phase diagram). Grey error bars are roughly evaluated from calculations on systems with  $L = 35$  and fixed  $\phi = 0$  (see Figs. 11 and 14 for details).

(see section IC for details). We focus on the differences and similarities between the deterministic bichromatic lattice potential and a truly random one, usually consisting in a random box distribution (RBD) and for which the phase diagrams without a trap are known [9, 10]. The main results are depicted on Fig. 1 which collects the phase diagrams for three typical densities as a function of the interaction strength  $U$  and the disorder potential strength  $V_2$ . A first interesting result is that a finite  $V_2 \geq 4$  is always required to stabilize the BG phase. We here precise that the term BG is used to name a localized phase with a zero one-particle gap, but the detailed features of the BG phase of the bichromatic potential differ from the usual RBD BG phase as discuss in what follows. Contrary to the RBD phase diagram, we argue, based on numerical evidence, that there is no intervening BG phase between the SF and the MI phase at  $n = 1$ , while an analytical reasoning is still missing. An incommensurate charge-density wave (ICDW) phase – referred to as the incommensurate band insulator (IBI) phase in Ref. 41 – emerges at finite  $V_2$  for a density  $n$  close to the irrational number  $r$ , the ratio of the employed lattice wave lengths, which characterizes the incommensurate potential. Lastly, we observe that the larger the density, the larger the extension of the SF phase is, which will be discussed later.

The paper is organized as follows: we first give in section I the conditions under which the hamiltonian describing the many-body physics simplifies into a simple lattice hamiltonian used for numerical calculations. We then discuss one of the strongest differences compared to a random box distribution which is the emergence of plateaus in the density-chemical potential curve (section II). We next discuss in section III the competition between the disorder potential and the interactions by computing the phase diagrams at integer density one and for a density for which an ICDW plateau occurs. Lastly, section IV is dedicated to the possible relevant

experimental probes of localization by focusing on the out-of-equilibrium dynamics of the system.

## I. THE BOSE-HUBBARD MODEL WITH AN INCOMMENSURATE SUPERLATTICE

### A. Energy scales hierarchy for the validity of the model

This section gives qualitative arguments on the hierarchy of energy scales which leads to a simple lattice hamiltonian which catches the physics of cold bosonic atoms experiencing two optical lattice potentials with wave vectors  $k_1, k_2$  and amplitudes  $V_1, V_2$ . The potential energy in a one-dimensional setup of two standing-waves is the Harper potential

$$V(x) = V_1 \cos^2(k_1 x) + V_2 \cos^2(k_2 x + \phi) \quad (1)$$

which is sketched in Fig. 2. A constant phase  $\phi$  is introduced to shift the second lattice w.r.t the other, and the wave vectors  $k_1$  and  $k_2$  can take any value. We work in the limit of a large depth  $V_1 \gg E_{r1}$  for which we can restrict ourselves to the lowest Bloch band ( $E_{r1} = (\hbar k_1)^2 / 2M$  is the recoil energy associated with the first laser and  $M$  is the mass of the atoms) and in a situation where one intensity is much larger than the other,  $V_1 \gg V_2$ . An exact derivation of the lattice hamiltonian parameters should resort to numerical calculations as described in Refs. 20, 41. Our motivation is to evaluate the physical effect of the perturbing potential to deduce the relative magnitudes of the different terms.

To proceed, we neglect the effect of the trap on the local chemical potential and displacements, meaning that we consider the realistic situation for the bulk physics with  $\lambda_1 \lambda_2 / |\lambda_1 - \lambda_2|, \lambda_1, \lambda_2 \ll 1/\sqrt{\omega}$  with  $\omega$  the trap frequency. If  $V_2 = 0$ , the effective model is the Bose-Hubbard model [11]

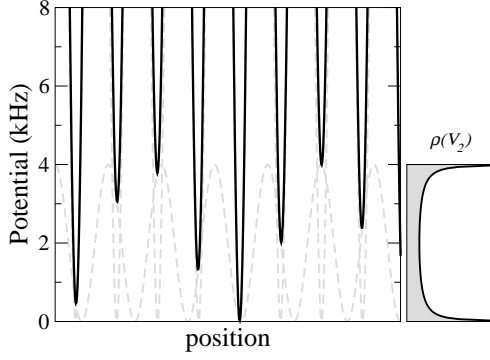


FIG. 2: The bichromatic potential (full line) with the same parameters as in the experiment of Ref. 22. Dashed lines show the two beating standing waves from which the bichromatic potential originates. We observe that not only the depths of the potential wells fluctuate but so do their positions and their width. The plot on the right-hand side shows the bounded distribution which behaves as  $1/\sqrt{x(V_2 - x)}$  and is thus peaked around 0 and  $V_2$ .

with hopping  $J_0$  and on-site interaction  $U_0$

$$\mathcal{H}_0 = -J_0 \sum_j [b_{j+1}^\dagger b_j + b_j^\dagger b_{j+1}] + U_0 \sum_j n_j(n_j - 1)/2. \quad (2)$$

$b_j^\dagger$  is the operator that creates a boson at site  $j$  corresponding to the minimum of the lattice potential. The local particle number operator reads  $n_j = b_j^\dagger b_j$ . The dependence of the parameters  $J_0$  and  $U_0$  upon  $V_1, E_{r1}, k_1$  and the scattering length  $a$  can be evaluated numerically or analytically in this limit [11]. We now qualitatively discuss the effect of  $V_2(x)$  to the lowest order in  $\varepsilon = V_2/V_1$ .

*Perturbation of the chemical potential* – First, to order zero in  $\varepsilon$ , the minima of  $V(x)$  are located at  $k_1 x_j = \pi j + \pi/2$  with  $j$  integer and  $\pi/2$  can be absorbed in the redefinition of  $\phi$ . Since  $V_1(x_j) = 0 + O(\varepsilon^2)$ , we have:

$$V(x_j) = V_2 \cos^2(r\pi j + \phi) = \varepsilon \frac{V_1}{2} [1 + \cos(2r\pi j + 2\phi)]$$

The important number which characterizes this bichromatic potential is the ratio of the wave vectors  $r = k_2/k_1$ . If  $r$  is a rational number  $p/q$ , the hamiltonian is  $q$ -periodic. For  $r$  irrational, it has no translational invariance and the  $V(x_j)$  can take any value in  $[0, V_2]$  in a deterministic way: the resulting bounded distribution is sketched in Fig. 2. The chemical potential thus shares features with a one-dimensional quasicrystal. The order of magnitude of the coefficient of this term is of course  $V_2 = \varepsilon V_1$ . Because of the factor  $V_1$ , this term can be larger than  $J_0$  or  $U_0$  even though  $\varepsilon \ll 1$ . Taking the parameters of Ref. 22, one finds that  $\varepsilon \simeq 0.003$ – $0.12$  while  $V_2/J_0 \simeq 2.6$ – $53.3$ .

*Perturbation of the hopping* – Even though it appears to be difficult to treat it exactly because one should know the non-trivial shape of the perturbed Wannier functions, we expect the hopping to be perturbed because of the displacement of the local minima and because tunneling depends exponentially on the distance. We only consider the term associated with the perturbation of the minima  $x_j$  and  $x_{j+1}$  and

assume a typical exponential dependence [11] for the hopping  $J_{j,j+1} \sim e^{-h(x_{j+1}-x_j)}$  with  $h = \frac{k_1}{2} \sqrt{\frac{V_1}{E_{r1}}}$ , valid for  $V_1 \gg E_{r1}$ . The modulation induces a slight fluctuation  $\delta x_j$  at site  $j$  which reads to the lowest order in  $\varepsilon$ :

$$\delta x_j = -\frac{1}{2k_1} \varepsilon r \sin(2r\pi j + 2\phi),$$

so that the distance between two neighboring sites is altered as:

$$x_{j+1} - x_j = \frac{\pi}{k_1} - \varepsilon \frac{r}{k_1} \sin(\pi r) \cos(r\pi(2j+1) + 2\phi).$$

Hence, we may write for this term to the lowest order in  $\varepsilon$ :

$$J_{j,j+1} = J_0 [1 + \varepsilon A \cos(r\pi(2j+1) + 2\phi)]$$

with, up to approximations,  $A = \sqrt{\frac{V_1}{E_{r1}}} \frac{r}{2} \sin(\pi r)$ . We write  $J_2 = \varepsilon A J_0$ . Even though  $A$  could be large because of  $\sqrt{V_1/E_{r1}}$ , the factor  $\varepsilon$  ensures that  $J_2$  can be made much smaller than  $J_0$ . More precisely, taking the parameters of Ref. 22 and using the above approximation, one finds  $J_2/J_0 \simeq 0.002$ – $0.1$ , the latter occurring for very large  $V_2$ , much larger than the ones used in this paper. Numerical calculations [20, 41] confirm that  $J_2$  can be neglected and we will use the shorter notation  $J \equiv J_0$  from now on. Another feature which results from this approximation is that the  $J_{j,j+1}$  have the same typical fluctuations  $\cos(2\pi r j)$  as the  $V(x_j)$  which is observed numerically in Ref. 41, yet for rather large  $\varepsilon$ .

*Perturbation of the local interaction* – In the deep well limit, the bare interaction  $U_0$  is obtained by the relation [11]:

$$U_0 = \sqrt{\frac{8}{\pi}} k_1 a E_{r1} \left( \frac{V_1}{E_{r1}} \right)^{3/4}$$

where  $a$  is the scattering length. Note that the ratio  $U_0/J_0 \sim \exp(2\sqrt{V_1/E_{r1}})$  increases exponentially with the lattice depth [11]. This result can be obtained by approximating the bottom of the cosines with a parabola and using gaussian Wannier functions as the simplest approximation. The fact that  $U_0$  increases with  $V_1$  simply corresponds to the squeezing of the parabola. This squeezing may also be changed at first order by  $V_2$ . To give a rough evaluation, we can compute the second derivative of Eq. (1) and obtain for the on-site interaction:

$$U_0 + U_2 \cos(2r\pi j + 2\phi) \text{ with } U_2 = \frac{3}{4} \varepsilon r^2 U_0.$$

Here again, since  $\varepsilon$  can be tuned to be very small, one can work within the  $U_2 \ll U_0$  regime. The perturbation of the onsite interaction can thus be neglected and we will use the shorter notation  $U \equiv U_0$  in the following. We also remark that the fluctuations of the local interactions have roughly the same cosine dependence as the chemical potential.

To conclude, in the deep well limit  $V_1 \gg E_{r1}$  the following hierarchy of energy scales

$$J_2, U_2 \ll U_0, J_0, V_2 \ll V_1$$

can be realized experimentally and the corresponding lattice model for the bichromatic optical lattice simplifies to:

$$\begin{aligned}\mathcal{H} = & -J \sum_j [b_{j+1}^\dagger b_j + \text{h.c.}] + U \sum_j n_j (n_j - 1)/2 \\ & + \frac{V_2}{2} \sum_j [1 + \cos(2r\pi j + 2\phi)] n_j \\ & + \frac{\omega^2}{2} \sum_j (j - j_0)^2 n_j\end{aligned}\quad (3)$$

with  $j_0 = \lfloor (L+1)/2 \rfloor$  the center of the trap.

We can briefly comment on the distribution of the on-site potential energies as it is the first difference with the RBD. We shall use the short-hand notation for the bichromatic potential  $V_2(x_j) \equiv V_j = V_2[1 + \cos(2r\pi j + 2\phi)]/2$ . The distribution of the  $V_j$  with an irrational  $r$  behaves as  $1/\sqrt{x(V_2 - x)}$  which diverges close to 0 and  $V_2$  and is symmetrical w.r.t.  $V_2/2$  (see Fig. 2) but is relatively flat at the center. Thus, this distribution qualitatively lies in between a RBD and a binary one. Its auto-correlation function reads:

$$\overline{V_j V_{j+d}} - \overline{V_j}^2 = (V_2)^2 \cos(2\pi r d + 2\phi)/8$$

where the over-bar means averaging over all sites  $j$ . The potential is thus deterministic and correlated. As sketched in Fig. 2 by black and dashed grey lines, wells develop over a characteristic length scale  $1/(1-r) \simeq 4.4$  sites which comes from the beating of the two periods 1 and  $r$  of the two lasers.

Working with finite systems raises the question of taking the thermodynamical limit. The system length  $L$  is given in units of the first lattice spacing  $\lambda_1/2$ . First, to what extent can an irrational number  $r$  be approximated by a rational number? This can be answered by looking at its continuous fraction decomposition [42] which gives the successive best rational approximations. From Ref. 22,  $r = 830.7/1076.8 = 0.77145245\dots$  is a realistic “irrational” parameter as 8307 and 10768 are coprimes. The successive best rational approximations are  $3/4, 7/9, 10/13, 17/22, 27/35, 908/1177, \dots$  which gives the lengths  $L = 13, 22, 35, 1177$  which best “fit” the potential for non-trapped systems. As  $27/35$  is already a fairly good approximation of the “irrational”  $r$  of the experiments, multiples of 35 like 70, 105, can be used as well. We will also use other lengths  $L$  and we have checked that the physics does not change qualitatively if the system size does not perfectly fit the potential. The fact that 35 is a rather large period ensures that  $r$  is not too close to a simple fraction which would induce strong commensurate effects on finite systems. In what follows, we chose to work with the experimental parameter  $r = 0.77145245$  as Roscilde did [41] to keep as close as possible to the experiments but we expect the general picture to remain true for any irrational number. Furthermore a phase shift  $\phi$  enters in the hamiltonian and, though we expect the potential to be self-averaging for fixed  $\phi$ , averaging over  $\phi$  can help recover the thermodynamical limit. This averaging will be denoted  $\langle \rangle_\phi$  in the following. As experimental set-ups generally consist in an assembly of one-dimensional cigar-shaped clouds with different lengths (see Fig. 3 of Ref. 23

for instance), clouds with different lengths would effectively experience a different phase shift  $\phi$ , even though  $\phi$  can be locked. However, we expect the trapped system to be less sensitive than a non-trapped one to these phase shift fluctuations.

The last crucial parameter in the physics of the system is the density which plays an important role as we will see. For a non-trapped system, we use the notation  $n = N/L$  with  $N$  the total number of bosons which is kept fixed as we will work in the canonical ensemble. For a trapped system, the local density varies as one moves away from the middle of the trap and the thermodynamical limit is recovered for  $\omega \rightarrow 0$  keeping  $N\sqrt{\omega}$  constant. Roscilde [41] gave a detailed analysis of the static properties in the presence of a trap. Our focus is more on the phase diagram of the model which is always understood to be in the thermodynamical limit. More details with respect to experimental probes will be given in section IV. All results of the paper are given at zero temperature.

## B. Low-energy approach: bosonization

We briefly review known results from the low-energy approach (close to a hydrodynamic description) which will be useful for the interpretation of the numerics and offer a complementary point of view on the physics. The low-energy physics of interacting bosons in 1D are described using Haldane’s harmonic fluid approach [43, 44, 45] in which the density operator is expanded as:

$$\rho(x) = \left[ n - \frac{1}{\pi} \nabla \phi(x) \right] \sum_{p=0, \pm 1, \pm 2, \dots} e^{ip(2\pi n x - 2\phi(x))} \quad (4)$$

where  $n$  is the boson density which encompasses the lattice spacing  $d$ . The effective hamiltonian of the system has generically a quadratic part which includes a kinetic energy term  $\sim \Pi^2$ , with  $\Pi = \frac{1}{\pi} \nabla \theta$  the conjugate field of  $\phi$  (the commutation relations  $[\phi(x), \Pi(x')] = i\delta(x - x')$  and  $[\theta(x), \frac{1}{\pi} \nabla \phi(x')] = i\delta(x - x')$  hold), and a density-density like interaction term  $\sim (\nabla \phi)^2$ . Two Luttinger parameters  $u$  and  $K$  give a simple parameterization of the quadratic part of the hamiltonian:

$$\mathcal{H} = \int \frac{dx}{2\pi} \left\{ uK(\pi\Pi)^2 + \frac{u}{K}(\nabla\phi)^2 \right\} \quad (5)$$

where  $u$  has the dimension of a velocity and  $K$  is dimensionless. For free bosons, only the first term remains which would formally correspond to the  $K \rightarrow \infty$  limit and  $u = \sqrt{n/\pi M}$  is the sound velocity. Taking into account a local interaction  $\frac{U}{2}\rho(x)^2$  like in the Bose-Hubbard model, the Luttinger parameters read  $u = \sqrt{nU/M}$  and  $K = \pi\sqrt{n/MU}$  in the limit  $U \ll J$ . When interactions are large, higher harmonics in the density operator have to be taken into account to describe correctly the local fluctuations and not only the long-distance ones. In the  $U = \infty$  limit, i.e. for hard-core bosons (HCB), one obtains  $K = 1$  as one would find for free fermions. The strong interaction, i.e. the second term in Eq. (5), acts as a Pauli exclusion term. We thus generically have for on-site

repulsive interactions  $1 \leq K < \infty$ . The effective hamiltonian (5) provides the general low-energy description of the SF phase which can undergo various instabilities.

By bosonizing the standard Bose-Hubbard model (2), commensurability effects can arise from the higher harmonics [45]:

$$\rho(x)^2 = n^2 + \frac{1}{\pi^2} (\nabla\phi)^2 + n^2 \sum_{p>1} \cos[2\pi p n x - 2p\phi(x)] + \dots$$

From studying the renormalization group (RG) flow equations, it is known that cosine terms such as

$$U \int dx \cos[2\pi p n x - 2p\phi(x)]$$

can lock the density field  $\phi$  and induce a commensurate-incommensurate transition [46, 47, 48] (C-IC) depending on the density and of  $K$ . Working at fixed density and varying interactions, such a term is relevant only if the density satisfies the commensurability condition  $pn = 1, 2, \dots$  and if  $K < K_c$  with  $K_c = 2/p^2$ . The opening of the gap follows a Kosterlitz-Thouless [49, 50, 51] (KT) law  $\Delta_c \sim \exp(-A/\sqrt{U - U^c})$  with  $A$  a constant and  $U^c$  the critical value. Working at fixed interaction and varying the density, the commensurate phase is obtained for  $K_c = 1/p^2$ . For instance, for  $p = 1$ , integer densities  $n = 1, 2, 3, \dots$  allow for a Mott phase for  $K$  below  $K_c = 2$ . For  $p = 2$ , charge-density wave phases can appear for half-integer densities but nearest-neighbor repulsion are required [45, 52, 53] to get  $K < 1$ . It is important to note that such cosine effective potential terms *effectively* arise from the interactions. The transition towards the charge density-wave (CDW) state with one atom every two sites [52] is associated with a spontaneous breaking of the translational symmetry. The other possibility to generate Mott phases is to *artificially* introduce a cosine chemical potential which directly couples to the density. Similarly, a CDW phase induced by an external potential is associated with an explicit breaking of the translational symmetry. This latter solution is possible in cold atoms by adding a superlattice.

*Effect of a superlattice periodic potential* – We first consider a cosine potential  $V_2(x) = \cos(Qx)$  which has only one Fourier component at wave vector  $Q = 2\pi r$  with  $r$  rational. The additional term reads

$$\int dx \cos(Qx) \rho(x) = \frac{1}{2} \int dx \cos[(2\pi n \pm Q)x - 2\phi(x)] + \dots$$

As seen previously, such terms may induce a C-IC transition when increasing  $V_2$  if the condition  $n \pm r \in \mathbb{Z}$  is satisfied. In particular, the superlattice potential can become relevant for the densities  $n = r, 1 - r, 1 + r, 2 - r, \dots$ . For higher harmonics  $p$ , the criteria would now be  $pn \pm r \in \mathbb{Z}$  but such plateaus might be more difficult to reach because smaller  $K$  are required, meaning stronger interactions. If the potential term is not relevant, the Luttinger parameter  $K$  is however renormalized to a lower value by the potential as it happens with interactions. Such commensurate potentials have for instance been studied in the context of Mott transitions [45] and of magnetization plateaus [54]. The physics of cold atoms and

the induced commensurate CDW phases was studied in details in Ref. 38. Vidal *et al.* [33, 34] generalized this result for irrational  $r$ . For the case of a quasiperiodic potential, the critical value  $K_c$  leading to the insulating phase can be smaller than 2 and the study of the RG flow equations found for a fermionic system  $K_c \simeq 1$ .

*Disorder with a random box distribution* – From Refs. [4, 5, 6], the main result is that the potential is relevant below the critical value  $K_c = 3/2$ , whatever the density. The resulting Bose-glass phase has no charge gap but exponentially decaying one-particle Green's function due to localization. The correlation length scales according to  $\xi \sim \exp(-A/(V_2 - V_2^c))$  where  $V_2^c$  is the critical value for the transition.

### C. Numerical methods

The hard-core bosons physics can be solved exactly using a Jordan-Wigner transformation which maps the model onto free fermions with boundary conditions that depend on the number of bosons. As the method has been widely described in the literature, we refer the reader to Refs. [41, 55]. This method is also used to investigate the out-of-equilibrium properties [55] of the cloud in section IV.

We used the DMRG algorithm [56, 57, 58] to treat the soft-core Bose-Hubbard model (3). For disordered systems, sweeping has proven to be particularly important to get reliable results [9, 59]. DMRG has also been used to investigate the physics of quasi-periodic electronic systems [60, 61]. Our implementation is based on a matrix-product state variational formulation [62] which enables us to start sweeping from any state. In practice, we have started from either a random or a classical state (where the particles are located according to the  $J = 0$  limit of the hamiltonian) contrary to the usual warm-up method. The algorithm is working in the canonical ensemble (fixed number of particles  $N$ ) and at zero temperature. This differs from the quantum Monte-Carlo method of Roscilde [41] which is most of the time working in the grand-canonical ensemble at a low but finite temperature. We mostly used 200 kept states with sometimes up to 400. The number of bosons allowed on-site was usually fixed to  $N^{\text{bos}} = 4$  but results for densities larger than one have also been checked with up to  $N^{\text{bos}} = 6$ . For  $U \geq 1$  and  $V_2 \leq 20$ , the classical distribution of particles does not have more than 4 bosons per sites.

A drawback of this variational method is the occasional tendency to get trapped in an excited (metastable) state with a slightly higher energy that is difficult to distinguish numerically from the groundstate. Indeed, the usual measures of the convergence of DMRG, the discarded weight and variance  $\langle (\mathcal{H} - E)^2 \rangle$  are very small for these states. Systematic tests have been carried out in the  $U \rightarrow \infty$  limit. Starting from the classical state improves convergence for small densities or close to one at large  $V_2$  as one would expect intuitively. Below  $V_2 \simeq 4$ , convergence is always good which can be related to the physics of the systems as the potential does not induce localization for this regime. For soft-core bosons we expect the enhancement of quantum fluctuations at finite  $U$  to help

the particles redistributing more easily. Such equilibration is rendered very difficult for HCB as for strong  $V_2$ , local densities can be very close to one. Most of the data have been done for  $U \lesssim V_2$ . Furthermore, relying on the variational principle, we can use the smallest of the two energies obtained from starting either from the classical or a random state. Lastly, the coherence of the results obtained from observables computed independently, like the correlation length and the one-particle gap (see section III), supports the good convergence of the algorithm.

## II. DENSITY PLATEAUS: MOTT AND INCOMMENSURATE BAND INSULATING PHASES

This section describes the relation between the density  $n$  and the chemical potential  $\mu$  for a non-trapped system. The chemical potential is computed via

$$\mu(N) = E_0(N) - E_0(N-1)$$

where  $E_0(N)$  is the ground-state energy with  $N$  bosons. If a plateau emerges in the  $n(\mu)$  curve, its width is directly related to the one-particle gap defined by

$$\begin{aligned} \Delta_c &= E_0(N+1) + E_0(N-1) - 2E_0(N) \\ &= \mu(N+1) - \mu(N) \end{aligned}$$

Lastly, the compressibility of the system  $\kappa = \partial n / \partial \mu$  is evaluated through its discretized expression as

$$\kappa^{-1} = L[E_0(N+1) + E_0(N-1) - 2E_0(N)] . \quad (6)$$

For a Luttinger liquid, the compressibility is simply related to the Luttinger parameters:

$$\kappa = \frac{K}{\pi u} . \quad (7)$$

The compressibility naturally vanishes in a plateau phase.

### A. Plateaus for hard-core bosons

Following Ref. 6, setting  $J = 0$  gives insights on the  $J \ll U$  physics. This gives the width  $U - \max(V_j) + \min(V_j)$  of the various Mott plateaus centered at  $\mu/U = 0.5, 1.5, 2.5, \dots$ . This is due to the fact that in the limit  $J = 0$  one can reorder the energies by increasing values and therefore the  $n(\mu)$  curve which is the integrated density of states is simply linear between Mott plateaus for the random box distribution and  $U > \max(V_j) - \min(V_j)$ . For a bichromatic lattice, we have  $\mu = V_2 \sin(\pi n/2)$ . What happens when  $J$  is small but finite? The density of states evolves smoothly with  $J$  for the random box distribution (see Fig. 3). For  $V_2 = 0$ , the bandwidth which develops between the Mott plateaus have width  $4J$  and a cosine relation can be observed [7] because Mott sub-bands with cosine dispersion are well separated. On the contrary, for the bichromatic lattice intermediate plateaus appear as soon as  $V_2$  is non-zero. This behavior is reminiscent of the situation

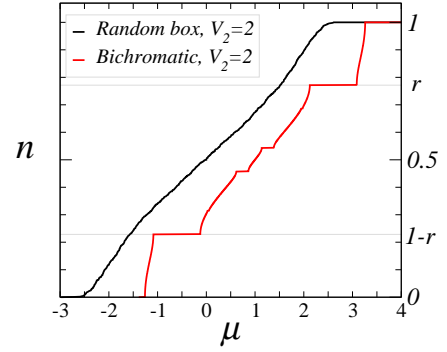


FIG. 3: (Color online) Comparing  $n(\mu)$  for a random and a bichromatic potential (irrational  $r$ ) for hard-core bosons. Plateaus open for the bichromatic potential, the main ones being at  $n = r$  and  $1 - r$ .

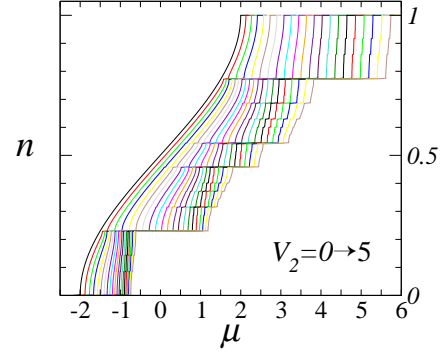


FIG. 4: (Color online) Opening of plateaus in the  $n(\mu)$  curves with  $V_2$  for hard-core bosons. Above the critical value  $V_2^c = 4$ , the curves acquire a devil's staircase-like behavior: plateaus become dense.

for rational  $r$  and was discussed extensively for free fermions which in our case would be equivalent to the HCB limit.

The energy spectrum and the wave function properties have been widely studied in the literature [24, 25, 26, 27, 28, 29, 30, 63]. It was shown that gaps open in the energy spectrum. If  $r$  is rational, there is a finite number of gaps. If  $r$  is irrational, there is an infinite number of gaps at large  $V_2$ , the width of which strongly depends on  $p$  and  $q$  if one writes  $n = p/q$  and gets larger as  $V_2$  increases. We here recall the method usually followed: these gaps are studied by  $m$  successive approximations  $r_m = p_m/q_m$  of the irrational number  $r$ . For a given  $m$ , the potential is  $q_m$  periodic and we can use Bloch's theorem on super-cells of length  $q_m$ . The one-particle Schrödinger equation of hamiltonian (3) reads:

$$-J(\psi_{j+1} + \psi_{j-1}) + [V_j - E]\psi_j = 0 . \quad (8)$$

Using  $V_{j+q_m} = V_j$  and Bloch's theorem  $\psi_{j+q_m} = e^{ikq_m}\psi_j$ , the spectrum is obtained by solving the determinant of size  $q_m$ :

$$\begin{vmatrix} V_1 - E & -J & -Je^{-ikq_m} \\ -J & V_2 - E & -J \\ & -J & \ddots & -J \\ -Je^{ikq_m} & -J & & V_{q_m} - E \end{vmatrix} = 0$$

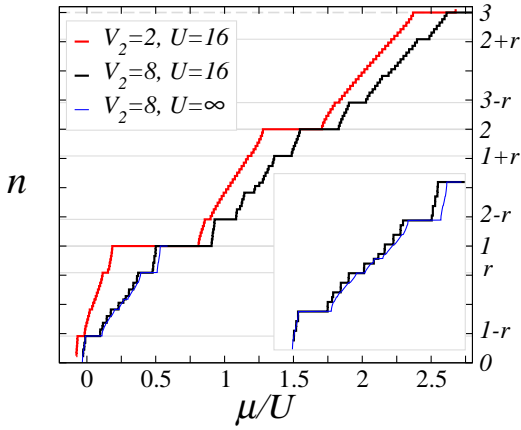


FIG. 5: (Color online)  $n(\mu)$  for soft-core bosons with a large interaction parameter  $U = 16$  at small and large  $V_2$  computed on a system with  $L = 35$  and a fixed phase-shift  $\phi = 0$ . *Inset*: curves at low density show the comparison between hard-core bosons and soft-core ones, which is good up to finite size effects.

For  $q_m = 2$ , this is the simple band folding mechanism which opens a gap at  $n = 1/2$ . More generally, at most  $q_m - 1$  gaps appear in the spectrum made of  $q_m$  bands  $\mathcal{E}_{1,\dots,q_m}(k)$  with  $k \in [-\pi/q_m, \pi/q_m]$ . Examples of effective dispersion relations can be found in Sec. IV. Fig. 4 displays the opening of the plateaus for HCB with  $V_2$ . The main plateaus develop for  $n = r, 1 - r$  as expected from the bosonization arguments of Sec. IB. These two plateaus open as soon as  $V_2$  is turned on since  $K(V_2 = 0) = 1 < K_c = 2$ .

### B. Plateaus for soft-core bosons

We now consider the case of a finite interaction  $U$ . First of all, the hard-core boson limit is likely to give the correct qualitative behavior for large  $U$ . Indeed, at low densities, an interaction  $U$  slightly larger than  $V_2$  might be sufficient to recover the HCB physics as multiple occupancies are already strongly suppressed. Densities larger than one are allowed for soft-core bosons. For large  $U$ , we expect to find plateaus in between each Mott plateaus. One would recover the hard-core bosons band folding mechanism inside each Mott sub-bands (or at least for the lowest ones). These simple observations are coherent with the large  $U$  numerical data displayed on Fig. 5. A comparison with HCB results is provided in the inset of Fig. 5 which proves that  $U = 16$  is sufficiently large to reproduce the HCB physics within the first three Mott sub-bands.

Fig. 6 gathers the results when  $U \leq V_2$ , unveiling a more surprising behavior. As discussed previously, we expect the HCB behavior to account for the low-density part of the curve, which is actually observed in the rather large width of the  $n = 1 - r$  plateau. For higher densities, a large compressible phase is obtained, manifested by the smooth increase of the density. From a phenomenological point of view, adding atoms fills the well minima. Since  $U$  is not too large, the effective potential coming from the combination of the interaction and the superlattice potential gets smoother and smoother.

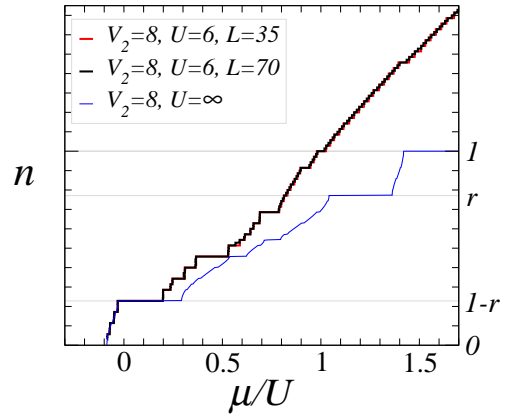


FIG. 6: (Color online) Plateaus with a large  $V_2 \sim U$ . Some of the largest plateaus found do not correspond to the hard-core boson limit. The two sizes give an idea of the (weak) finite size effects.

Consequently, the associated gain in kinetic energy favors a compressible and actually a superfluid state as we will see in Sec. III H where delocalization by increasing the density is discussed. In between those two regimes, the behavior is non-trivial. Strikingly, some plateaus existing in the HCB limit totally disappear, like the  $n = r$  plateau, while others acquire a larger width. Having gaps whose size increases when interactions are reduced is something rather counter-intuitive. These plateaus result from the interplay of the potential and the interactions. A real-space picture was given by Roscilde [41] following a random atomic limit: considering wells of typical size  $1/(1-r)$  separately, the fine structure of the energy levels for each number of atoms inside the wells depends strongly on  $U, V_2$  and also on  $J$ . Connecting wells with  $J$  allows for the computation of the integrated density of states which is  $n(\mu)$ . Since the observed plateaus stem from the interplay of the interactions and the potential, we might call the corresponding plateau phase an incommensurate charge density-wave phase. They appear to be the extension of both the Mott and the incommensurate HCB phases at smaller  $U$ .

### III. LOCALIZATION INDUCED BY INTERACTIONS OR DISORDER: MOTT, ICDW AND BOSE-GLASS PHASES

We have seen that contrary to the standard random box situation, there is not only one phase (either the BG or the SF) between the MI phases but a succession of phase transitions as the chemical potential is increased. We now describe more precisely the nature of these phases by computing various observables at fixed density and varying the two competing parameters  $V_2$  and  $U$ . These phase diagrams were first sketched numerically in Refs. [35, 36, 37] but on very small systems and without a discussion of the boundaries and the nature of the transitions. We here provide a more precise determination, in particular by using scaling over different sizes and averaging over  $\phi$  when necessary.



### A. Observables

In addition to the compressibility, we need further observables to sort out the different phases realized in the bichromatic set-up. The first natural one is the superfluid density  $\rho_s$ . It can be computed using twisted boundary conditions:

$$\rho_s = 2\pi L \frac{E_0^{\text{apbc}} - E_0^{\text{pbc}}}{\pi^2} \quad (9)$$

where the ground-state energies are computed for periodic (pbc) and anti-periodic (apbc) boundary conditions. With this definition,  $\rho_s$  actually matches the superfluid stiffness. Other definitions [9] have the density of particles  $n$  as a prefactor. The superfluid density is zero for the BG, ICDW and MI phases and finite only for the SF phases. In a Luttinger liquid, the superfluid density is directly related to the Luttinger parameters through

$$\rho_s = uK. \quad (10)$$

Combined with Eq. (7),  $K$  can then be computed using  $K = \sqrt{\pi\rho_s\hbar}$ . This numerical evaluation only requires the calculation of energies.  $K$  can be independently extracted from correlation functions. For instance, the one-particle density-matrix or bosonic Green's function reads  $\langle b_i^\dagger b_j \rangle$  where  $\langle \rangle$  indicates the expectation value in the ground-state. Following Ref. 64, we extract the contribution of the phase  $\theta(x)$  fluctuations by dividing it by the local inhomogeneous densities  $n_i$ :

$$G(|i-j|) = \frac{\langle b_i^\dagger b_j \rangle}{\sqrt{n_i n_j}}. \quad (11)$$

The motivation for this renormalization comes from the remark that the boson creation operator  $b_i = \sqrt{\rho(x_i)}e^{-i\theta(x_i)}$ , and the fact that the correlator which features superfluid properties in bosonization is  $\langle e^{i\theta(x_i)}e^{-i\theta(x_j)} \rangle$ . For a translationally invariant model, both definitions only differ by a constant factor. Since there is no translational invariance, one must likewise average correlations over all couples of points with same distance  $x = |i-j|$  to obtain a smooth behavior for this correlation. A typical plot is given in Fig. 19. In the case of the BG, ICDW or MI phases, the Green's function must decay exponentially  $G(x) \propto e^{-x/\xi}$ . For the Mott phase, the correlation length  $\xi$  goes as the inverse charge gap  $\xi \sim 1/\Delta_c$ . An effective correlation length can also be computed on a finite system using [52]:

$$\xi^2(L) = \frac{\sum_x x^2 G(x)}{\sum_x G(x)}. \quad (12)$$

This gives a correct estimate of the correlation length for the localized phases in the thermodynamical limit up to a factor  $\sqrt{2}$ . A divergence of  $\xi$  with  $L$  signals a superfluid state in which the asymptotic behavior of the Green's function is algebraic with an exponent controlled only by the parameter  $K$

$$G(x) \propto \frac{1}{x^{1/2K}}. \quad (13)$$

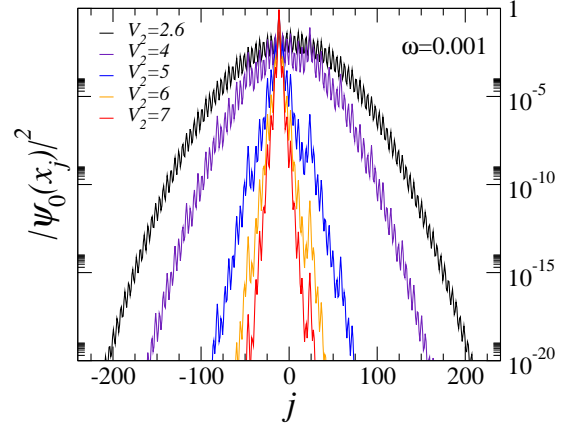


FIG. 7: (Color online) Ground-state wave function of the lattice model (3) with a smooth trap but no interaction for increasing perturbing potential  $V_2$ . There is a crossover from a gaussian wave function (log scale) to an exponential one. Note that the maximum of the wave function in presence of strong  $V_2$  is not centered at the middle of the trap.

This allows for the evaluation of  $K$  by using an accurate fitting procedure on a finite system with open boundary conditions. This is briefly described in Appendix A.

Characterizing the Bose condensation of the cloud is often done by looking at the condensate fraction  $f_c$ . It is usually computed on finite clusters as the largest eigenvalue of the matrix  $\rho_{ij} = \langle b_j^\dagger b_i \rangle$ . No average over sites nor normalization by the local density is performed here. The largest possible value  $f_c$  can reach is the number of bosons  $N$ . In the limit of HCB, quasi-condensation results in the scaling  $f_c(N) \propto \sqrt{N}$ . A finite  $f_c$  is a feature of either the BG, the ICDW or the MI phase. Experimentally, time-of-flight measurements are related to the Fourier transform of  $\rho_{ij}$ , namely

$$n(k) = \frac{1}{L} \sum_{lm} e^{ik(l-m)} \rho_{lm}. \quad (14)$$

Coherence of the quantum gas is deduced from the appearance of a narrow central peak  $n(k=0)$ .

### B. Localization of free bosons

We start with the simplest situation of free bosons, the  $U = 0$  limit, in which all bosons lie in the ground-state single particle wave function  $|\psi_0\rangle$ . In Fig. 1 of Ref. 22, the structure of the trapped wave function is obtained from the Gross-Pitaevskii equation. Similar results are found for the *lattice* model (3) as shown in Fig. 7 which displays the qualitative change of shape from a gaussian to an exponential structure. In order to quantify the localization transition of a *single-particle* wave function  $|\psi\rangle$ , one can use the inverse participation ratio which is usually defined as

$$I(\psi) = \sum_j |\langle \psi | j \rangle|^4. \quad (15)$$



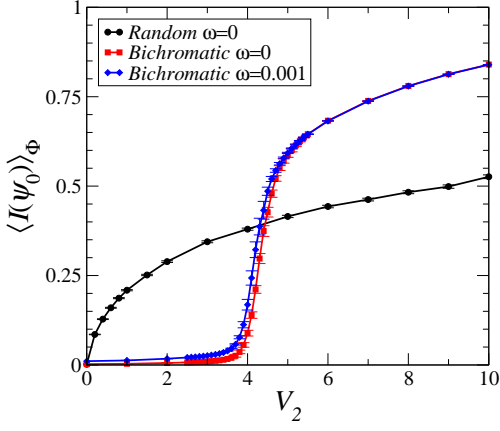


FIG. 8: (Color online) The averaged inverse participation ratio  $\langle I(\psi_0) \rangle_\phi$  as a function of  $V_2$  for a bichromatic lattice and a random box distribution. There is a sharp transition at  $V_2^c = 4$  in the thermodynamical limit ( $L = 420$  for  $\omega = 0$ ). A similar sharp transition is also found for the system with a smooth trap.

$|j\rangle$  is the state at site  $j$  in the real space basis. In the thermodynamical limit,  $I(\psi)$  goes to zero for a delocalized state with a typical scaling  $1/L$  or  $\sqrt{\omega}$  for respectively a non-trapped and a trapped system, while it remains constant for a localized wave function. Based on an exact duality transformation of the one-particle Schrödinger equation (8), the localization of the wave function has been conjectured by Aubry and André [24] to happen at the critical value  $V_2^c = 4$ . This conjecture is illustrated in Fig. 8 which displays  $\langle I(\psi_0) \rangle_\phi$  as a function of  $V_2$ . In comparison with the RBD evolution, the bichromatic set-up displays a sharp transition even for a finite trap frequency provided it is small enough. For the RBD, localization occurs as soon as  $V_2 \neq 0$  [3] with a typical scaling  $I(\psi_0) \sim \sqrt{V_2}$ .

### C. Localization of hard-core bosons

We have seen that plateaus emerge in the  $n(\mu)$  curve as soon as  $V_2$  is turned on and that the spectrum is point-like above  $V_2^c = 4$ . The extension of the wave functions is related to the nature of the energy spectrum and it was shown [24, 30] that all wave-functions are extended below  $V_2^c$  while they are all localized above. Consequently, we expect the HCB to localize above  $V_2^c$ , whatever the density. Below, HCB can be either in a SF or in an ICDW state. To illustrate this situation, we give the behavior of the Luttinger exponent  $K$  in Fig. 9. It nicely shows that  $K = 1$  within superfluid phases as expected for HCB but vanishes (up to finite size effects) for the densities corresponding to the ICDW phases, the main ones being located at  $n = r$  and  $1 - r$ . Many gaps develop as the critical point is approached and the shrinking of the bands renders difficult the low-energy approximation and calculation of  $K$  close to this point.

As a partial conclusion, the two limiting cases  $U = 0$  and  $U = \infty$  of the  $(U, V_2)$  phase diagrams of Fig. 1 are depicted as follow: (i) for a generic density  $n$  (meaning which does not lie at an ICDW plateau) and also for the  $U = 0$  limit whatever

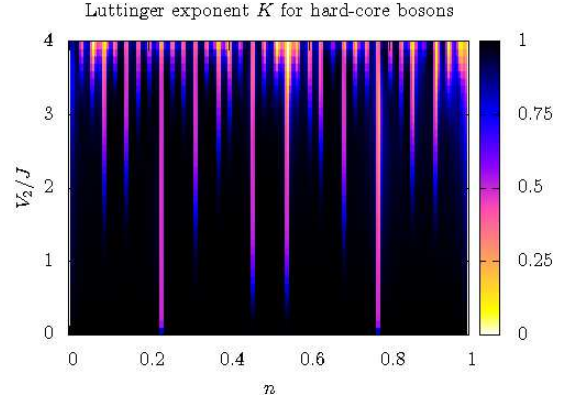


FIG. 9: (Color online) The Luttinger parameter  $K$  for hard-core bosons as a function of  $V_2$  and the density  $n$  on a *finite* system with  $L = 175$  for an irrational  $r = 0.7714 \dots$ . Strictly speaking  $K$  should be equal to 1 in all superfluid phases and 0 in the gapped phases. Up to finite size effects, vertical bands manifest the successive openings of gaps as  $V_2$  is increased.

the density, the system remains superfluid for  $V_2 < 4$  and localizes in a BG phase for  $V_2 > 4$  with a correlation length which behaves according [24, 25, 28] to  $\xi^{-1} \sim \ln(V_2/4)$ , (ii) for a density close to a plateau phase (for instance  $n = r$  or  $1 - r$ ) and  $U = \infty$ , there is a transition towards an ICDW phase for a critical value of  $V_2$  which is below 4 and equal to 0 for  $n = r$  or  $1 - r$ , (iii) for the commensurate integer density  $n = 1$  and  $U = \infty$ , the system remains in the MI phase ground-state for any  $V_2$ .

### D. The superfluid – Bose glass transition for soft-core bosons

We first discuss the direct transition from the SF to the BG phase which occurs for a generic density by increasing the strength of the potential  $V_2$ . Fig. 10 provides the evolution of the Green's function  $G(x)$  showing the Anderson-like localization transition. First, a finite “disorder” strength with a critical value  $V_2^c \simeq 6.9$  is necessary to obtain exponentially decaying correlations. This value is larger than the  $U = 0$  and  $U = \infty$  limits; interactions have a delocalization effect on the BG phase similarly to the RBD box results. Interestingly, computing the Luttinger exponent from the correlations shows that the critical value  $K_c$  at the transition is smaller than the RBD result  $3/2$ . The scaling properties of the transition thus differ from the standard SF-BG transition. Finding a  $K_c$  smaller than the RBD result for the Harper potential is well compatible with the analytical finding for  $K$  found for the Fibonacci potential in Ref. 33, 34.

To proceed with the discussion of the competition between interactions and the disordered potential, we have computed with DMRG the phase diagrams of the system in the three generic cases  $n = 1$  (competition between the SF, Mott and BG phases),  $n \simeq r$  (competition between the SF, ICDW and BG phases), and lastly  $n = 0.5$  (competition between the SF and BG phases only). The summary of the phase diagrams is given in Fig. 1.

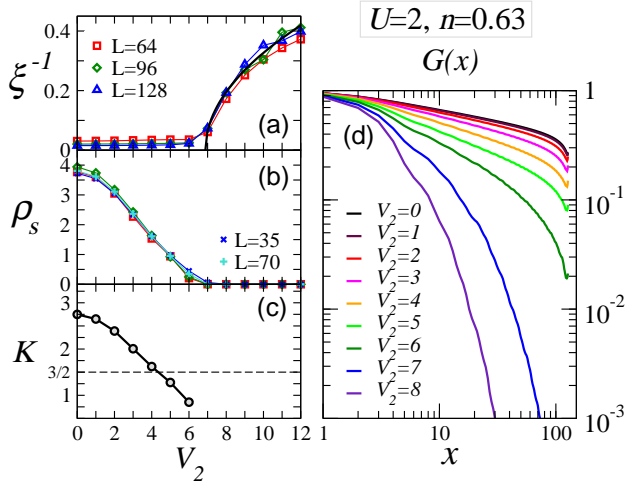


FIG. 10: (Color online) *Superfluid-Bose glass localization transition.* The parameters  $U = 2$  and  $n = 0.63$  are such that the system is in the superfluid phase at  $V_2 = 0$ . (a) The inverse correlation length scales roughly as  $\sqrt{V_2 - V_2^c}$  where  $V_2^c = 6.9$  is much larger than the non-interacting critical value  $V_2^c = 4$ . Below  $V_2^c$ , we have the scaling  $\xi \sim L$  typical of a superfluid state (b)  $\rho_s$  gives an independent determination of the transition. (c) Evolution of the Luttinger exponent  $K$  as a function of  $V_2$ . The dashed line displays the RBD result  $K_c = 3/2$ . (d) averaged one-particle density-matrix  $G(x)$  for increasing  $V_2$  showing the transition from an algebraic to an exponential behavior.

### E. Phase diagram at $n = 1$

All relevant observables to construct the phase diagram as a function of the interaction  $U$  and the potential depth  $V_2$  are reported in Fig. 11 for the integer density  $n = 1$ . The Mott phase is characterized by a finite gap  $\Delta_c \sim 1/\xi$ , a zero SF density and condensate fraction. It emerges at the bottom right corner above the critical value [52]  $U^c \simeq 3.3$  for  $V_2 = 0$ . We observe that  $U^c$  increases with  $V_2$  as for the RBD, meaning that  $V_2$  destabilizes the Mott phase as one can understand from simple local on-site energies arguments: the disorder reduces the minimum one-particle energy gap in the atomic limit. The BG phase has exponentially decaying correlations, a zero SF density and a non-diverging condensate fraction but no gap. It occurs generically for large  $V_2$  region of the  $V_2 > U$  half-part of the phase diagram. The SF phase has a finite SF density but no gap and algebraic correlations. It generically emerges at low  $U$  and low  $V_2$  and surprisingly extends into a hand print like pattern. A small one-particle charge gap is observed for large  $U$  and large  $V_2$ . A scaling and averaging (see Fig. 13) of this gap shows that is quite small in the thermodynamical limit (compare for instance to the Mott gap). Furthermore, it does not show up for the same phase diagram on a system with  $L = 30$ . We thus conclude that this small gap is a finite size effect.

*Superfluid-Mott transition and intervening Bose-glass phase* – An important question is whether the SF and Mott touch each other at small but finite  $V_2$ . In other words, is there always an intervening BG phase between the SF and the MI

phases as for the RBD [9, 10]? For the bichromatic potential, we however have reasons to think that small  $V_2$  might not be as relevant as for true disorder since a large critical value exists for both hard-core and free bosons. To address this issue numerically, we have compared the scaling of the most relevant observables for the known case  $V_2 = 0$  and for  $V_2 = 2$  (see Fig. 12). When  $V_2 = 0$ , the SF-MI transition is of the Kosterlitz-Thouless type leading to an opening of the one-particle gap  $\Delta_c \propto \exp(-A/\sqrt{U - U^c})$  above the critical value  $U^c$ , with  $A$  a constant. Such an opening gives a good fit to the extrapolated data (see Fig. 12) but does not precisely give  $U_c$ . Finding  $U_c$  is rather achieved by using the weak-coupling RG result  $K_c = 2$  for the KT transition. Fig. 12 shows that  $U^c \simeq 3.3 \pm 0.1$  for  $V_2 = 0$  in agreement with results of Ref. 52. Within error bars, the scalings of the superfluid stiffness  $\rho_s$  and correlation length also agree with this critical point. Note that because of the very slow opening of the one-particle gap in a KT transition, the correlation length and superfluid density show much smoother finite size effects than for the SF-BG transition illustrated in Fig. 10. For  $V_2 = 2$ , if a BG is present in between the SF and MI phase, the one-particle gap  $\Delta_c$  should open after the superfluid stiffness scales to zero. Up to numerical accuracy, data are consistent with a direct SF-MI transition of the KT type with a slightly larger critical interaction  $U^c \simeq 3.6 \pm 0.1$ . We observed that averaging over  $\phi$  is needed to ensure a good crossing of the scaling curves (see insets of Fig. 12). Note that for the RBD situation,  $V_2 = 2$  would correspond to a disorder amplitude  $\Delta = 1$  in Ref. 9 (or  $\Delta = 0.5$  in Ref. 10) for which the BG phase already has a significant width.

*Superfluid-Bose Glass transition* – We now turn to the discussion of the contour of the SF-BG transition which displays a hand print pattern. First, contrary to the RBD, the BG phase emerges only above  $V_2^c = 4$  and for much larger values for small  $U$ . Secondly,  $V_2^c$  increases with  $U$  at small  $U$  which is the similar delocalization by interactions effect observed in the RBD case. Similarly to what was found in Fig. 10, the inverse correlation length has a power-law behavior above the critical point with an exponent smaller than  $3/2$ . The convexity of the SF phase contours changes contrary to the RBD phase diagram, leading to this hand print pattern. To understand if these reentrances of the SF phase inside the BG phase are not a finite size effect and remain after averaging over  $\phi$ , we give the averaged  $\langle \rho_s \rangle_\phi$  and  $\langle \xi \rangle_\phi$  for various system sizes in Fig. 13. Data for  $\xi$  and  $\rho_s$  suggest two reentrances of the SF phase and in particular, a sharp but clear one close to the transition to the MI phase. The  $U = V_2$  line corresponds to the “transition” between the MI and BG phases in the atomic limit. It gives a rough estimate for the extension of a SF phase at large  $U$  and  $V_2$  which does not occur for the RBD situation. A similar emergence of the superfluid phase around the atomic limit was found in Ref. 38 for the case of a commensurate potential where the SF phase competes a CDW and a MI phase. On Fig. 13, the intermediate localized phase between the two SF reentrances displays a small gap which does not satisfy the behavior  $\xi \sim 1/\Delta$  as for the MI phase. This phase could have a finite gap but we observe that if so, it cannot be distinguished from finite size effects.

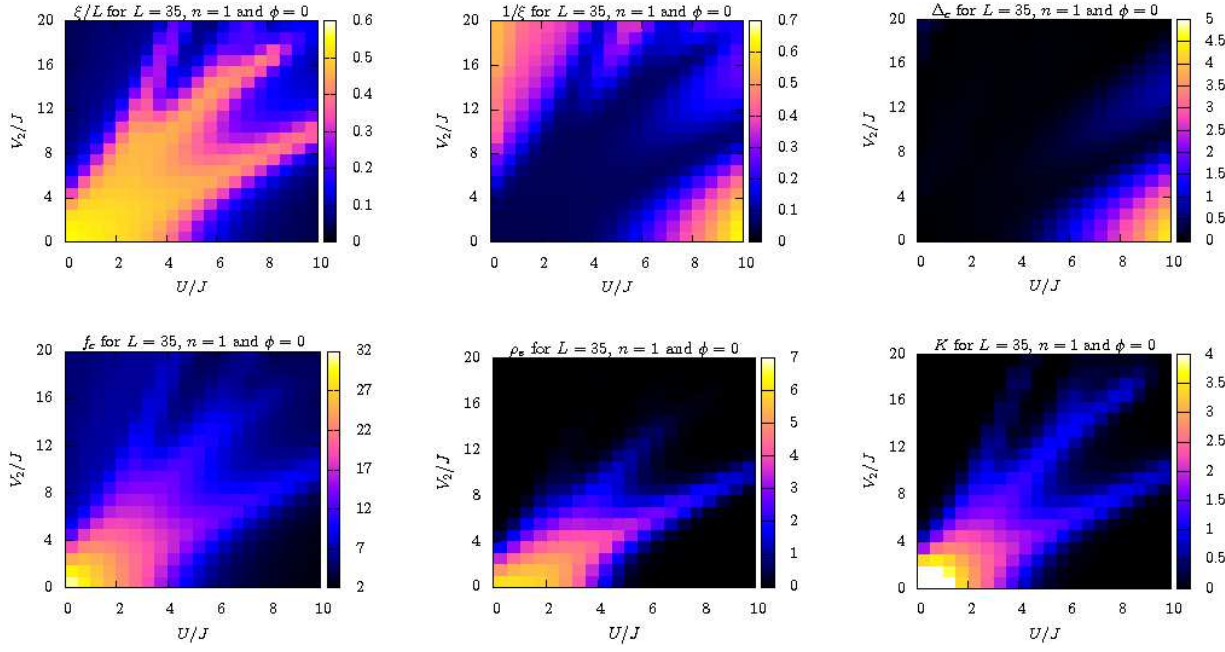


FIG. 11: (Color online) *Phase diagram for  $n = 1$ .* Observables are computed with DMRG for a system with  $L = 35$  and fixed phase-shift  $\phi = 0$  as a function of  $U$  and  $V_2$ . The  $V_2 = 0$  line shows the Mott transition at  $U^c = 3.3$  while the  $U = 0$  line shows the free boson localization transition around  $V_2^c = 4$ . The Mott insulating phase gets qualitatively delocalized as  $V_2$  increases for  $U$  not too large. Increasing  $U$  delocalizes the BG phase  $V_2$  if not too large.

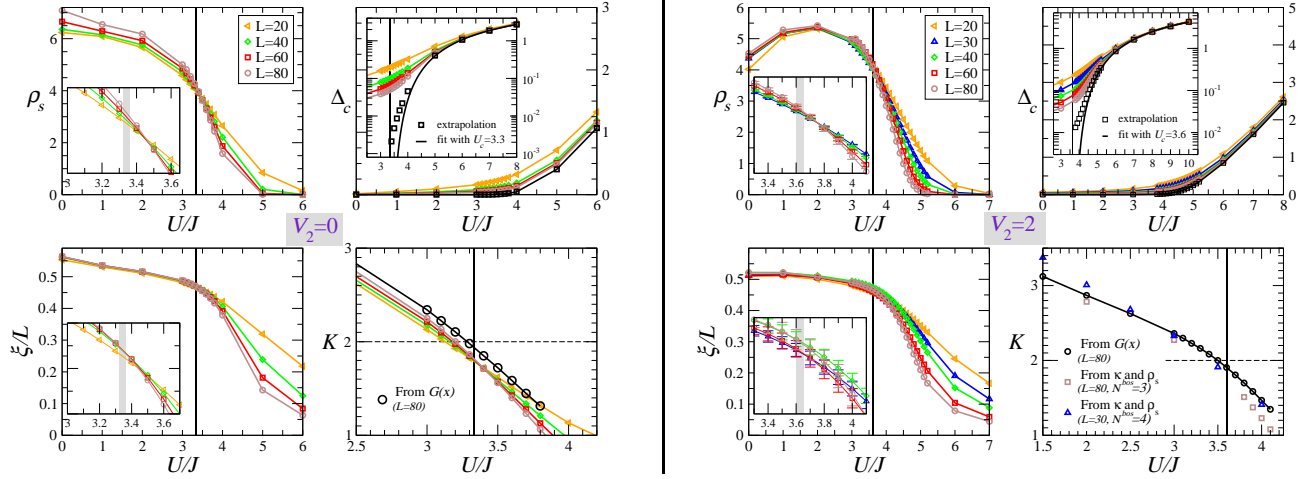


FIG. 12: (Color online) *Superfluid-Mott insulator transition for  $n = 1$ .* Cuts along the  $U$ -axis for  $V_2 = 0$  and 2. **Left:** data giving similar results to those of Ref. 52 (the vertical bar being  $U^c \simeq 3.33 \pm 0.1$ ). Data are computed with  $N^{bos} = 4$  and the Luttinger exponent  $K$  is determined using either  $\rho_s$  and  $\kappa$  or  $G(x)$  (see Sec. III A). Scaling of  $\rho_s$ ,  $\xi/L$  and the criteria  $K_c = 2$  gives the same critical point within error bars. The scaling of the condensate fraction (not shown) is not simple at the transition and the HCB scaling  $f_c \propto \sqrt{L}$  does not hold. **Right:** the same observables for  $V_2 = 2$  and  $N^{bos} = 3$ . Insets show scaling behavior for  $\rho_s$  and  $\xi/L$  after averaging over several different  $\phi$ . A critical point  $U^c \simeq 3.6 \pm 0.1$  is found which corresponds to  $K_c \simeq 2$ . Furthermore, the one-particle gap (not averaged over  $\phi$ ) is best fitted by a Kosterlitz-Thouless opening (we fixed  $U^c = 3.6$  for the fit). Up to numerical precision, we infer from these results that the transition is direct between the SF and the MI phases without intervening BG phase.

#### F. Phase diagram close to the density $n = r$

A density which satisfies the criteria  $n \simeq r$  allows for the realization of an ICDW phase which competes with the SF and BG phases. The  $(U, V_2)$  map of the observables is given

in Fig. 14. The ICDW phase has a finite gap and exponentially decaying correlations as the MI phase. Similar qualitative features are found with the ICDW phase replacing the MI phase. However, a finite  $V_2$  is of course required to stabilize the ICDW phase contrary to the MI phase. Secondly, a finite



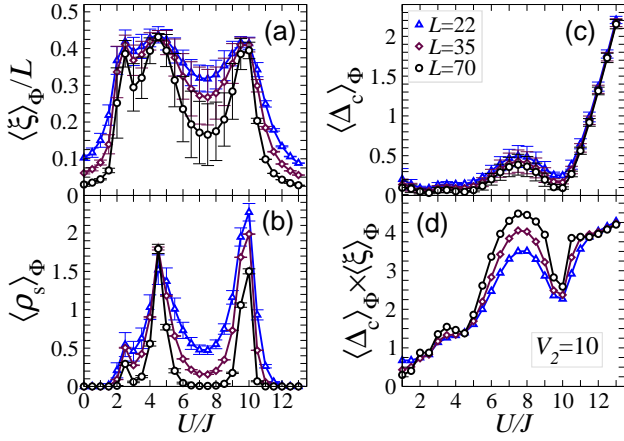


FIG. 13: (Color online) *Reentrances of the SF phase with increasing interactions.* Cut at  $V_2 = 10$  in the phase diagram of Fig. 11. Error bars are related to the average over the phase-shift  $\phi$  (about twenty realizations). The scalings of the correlation length (a) and the superfluid density (b) suggest two reentrances of the SF phase as  $U$  is increased. In between, a localized phase is found and a MI phase is obtained at large  $U$  according to the gap (c). In the intermediate BG phase (for  $U \simeq 6-9$ ), a small gap is found, but for the chosen sizes, the scaling  $\xi \sim 1/\Delta$  shown in (d) seems to be satisfied only in the MI phase.

$V_2$  is needed to stabilize the BG phase. As a consequence, the SF phase extends to large  $U$  close to the  $V_2 = 0$  line. As discussed in section II, the ICDW is a new feature compared with the RBD phase diagram given in Ref. 9, 10 for  $n = 0.5$ . Similar reentrances of the SF phase into the BG phase are found at fixed  $V_2$  and increasing  $U$ . The  $U = \infty$  line of the phase diagram would give an ICDW phase everywhere except for  $V_2 = 0$  since the  $n = r$  plateau occurs as soon as  $V_2$  is finite in the HCB limit.

#### G. Phase diagram for a generic density $n = 1/2$

Lastly, the phase diagram for a generic density  $n = 1/2$  (meaning no competing ICDW nor MI phase) has been computed (data not shown, see phase diagram in Fig. 1) to discuss the sole competition between the SF and BG phases. Similar observables suggest that  $\Delta_c$  remains zero for the whole parameter range while the BG is bounded by the  $V_2 = 4$  line and the SF phase extends a little bit inside the BG phase for small  $U$ . However, critical values  $V_2^c$  for the SF-BG transition are found to be smaller than for  $n = r$ , itself smaller than for  $n = 1$ . The same qualitative argument claiming that the lower the density, the closer the physics is to the HCB can be put forward. The SF region extends with the density of the system. This observation will be now more precisely discussed.

#### H. Delocalization via increasing the density of bosons

An orthogonal approach to these  $(U, V_2)$  phase diagrams is to keep  $U$  and  $V_2$  constant and to look at the observables as

a function of the density  $n$ . Experimentally, Lye *et al.* [22] observed from dipole oscillations measurements a delocalization transition by increasing the number of particles. We now address the non-trivial case of  $U \sim V_2$  by setting  $U = 6$  and  $V_2 = 8$  corresponding to the parameters of the  $n(\mu)$  curve of Fig. 6. Results for the same observables as for the phase diagrams are plotted in Fig. 15. We found transitions between the three different phases BG, ICDW and SF. At low densities, double occupation for bosons is strongly suppressed because of the finite  $U$ . Consequently, the behavior is qualitatively the one HCB would have:  $V_2$  being larger than 4, localization exists at low densities. The superfluid density, correlation length and one-particle gap confirm the presence of the BG phase. At large densities, a SF emerges which is something well-known without disorder because the lobes of the Mott phases shrink at large densities [52]. In addition, the disordered potential has a tendency to reduce the size of the Mott phases as we have seen. Very qualitatively, some particles fill the wells of the disorder potential so that the remaining ones feel a smoother effective potential allowing for a gain in kinetic energy leading to superfluidity. This behavior for an irrational  $r$  is qualitatively similar to what was observed for a rational  $r$  (see Fig. 23 of Ref. 38) except that no BG, but a “weakly superfluid” phase is realized in this latter case. Besides this sharp BG-SF transition, peaks in the one-particle gap  $\Delta_c$  uncover the presence of ICDW phases within both the BG and the SF phases. These phases naturally correspond to the plateaus in Fig. 6.

### IV. PROBING THE BOSE-GLASS PHASE WITH OUT-OF-EQUILIBRIUM DYNAMICS

The question of probing experimentally the BG phase with respect to the other possible phases is particularly important. First, the simplest observable obtained after time-of-flight measurements is related to the momentum distribution of the atoms  $n(k)$ . This measure helps to distinguish between coherent and incoherent phases by looking in particular at the  $k = 0$  peak. A sharp and high peak is the signature of a coherent phase, the superfluid phase. Because of short-range correlations, both the MI and the BG phases will give a much smaller peak broadened with typical width  $\xi^{-1}$ . Fig. 16 displays  $n(k)$  in the BG at small  $U$ . In addition to the central peak, satellites peaks at  $k = \pm 2\pi(1 - r)$  emerge as a signature of the underlying superlattice. However, in the experiment pictures, the Wannier envelope and the broadening of the peaks due to scattering events during the time of flight will change the observed shape. It is expected that the additional satellite peaks are too small to be experimentally resolved and are washed out if either  $V_2$  and/or  $U$  are too large. Thus,  $n(k)$  can only be used to distinguish the superfluid from the Bose-glass or Mott insulating phases. However, it would not help to distinguish the MI from the BG phase. Refs. 35, 41 found a similar behavior and for the second a non-monotonic evolution of the central peak  $n(k = 0)$  with increasing  $V_2$ . The reinforcement of the superfluidity while increasing  $V_2$  at fixed  $U$  must be reminiscent of the MI-SF-BG transitions of the phase dia-

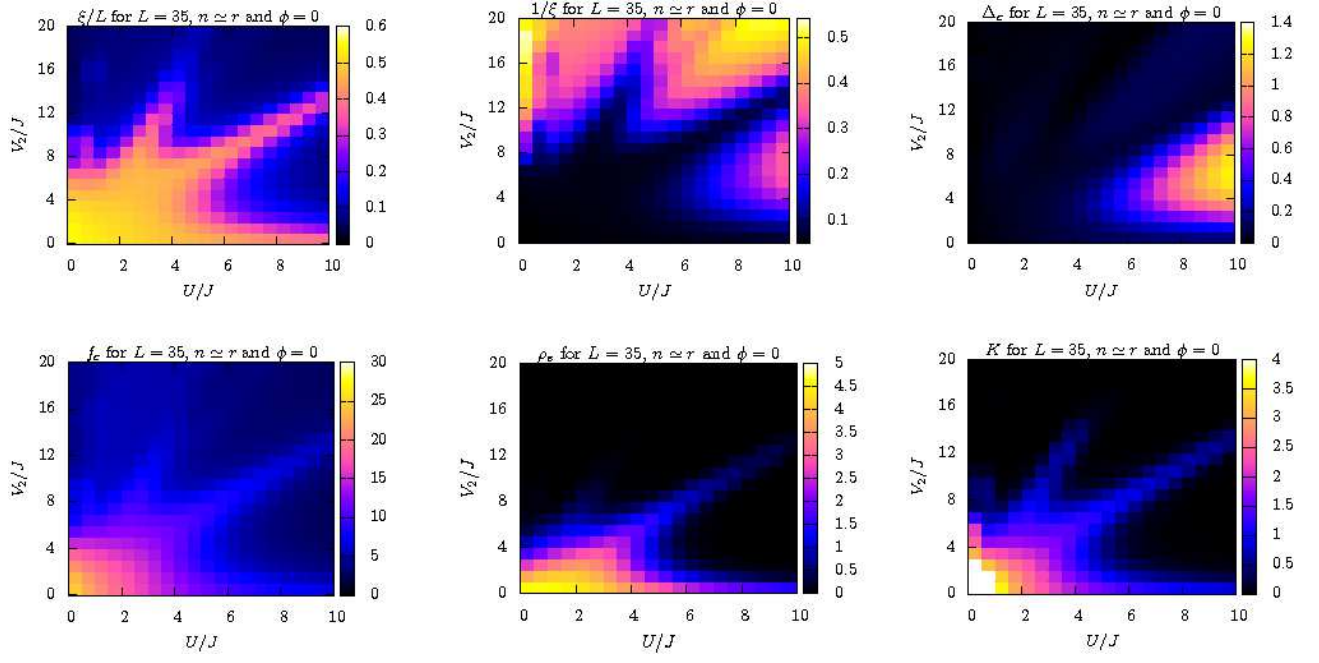


FIG. 14: (Color online) *Phase diagram for  $n \simeq r$ .* Observables are computed on a system with fixed size  $L = 35$  and fixed phase-shift  $\phi = 0$ . A large ICDW phase emerges at large  $U$ . A finite  $V_2$  is required to stabilize it. The SF phase extends along the  $V_2 = 0$  contrary to the phase diagram with  $n = 1$ .

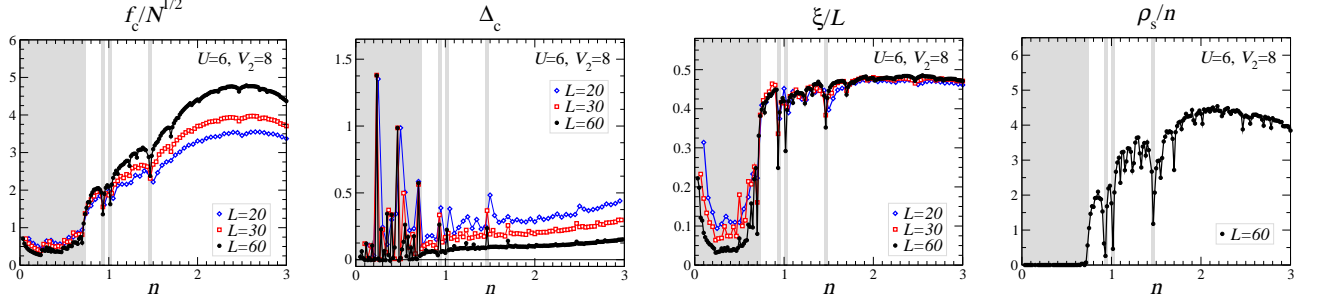


FIG. 15: (Color online) *Delocalization by increasing the number of particles.* Observables for increasing density when  $V_2 \simeq U$  (same parameters as in Fig. 6). There is a delocalization transition with increasing density. A few ICDW phases can be seen at intermediate fillings. Grey areas denote the localized regions (either BG or ICDW). The weakening of the superfluidity at large density might be an artefact of the cut-off in the number of bosons kept per site which is here  $N^{bos} = 4$ .

grams of Fig. 1. Noise correlations could be a better way to compare a MI to a BG phase [41].

As usually done in experiments [12, 13, 14, 15, 17, 22], transport measurements are better to probe the BG phase. Exact results for the long times out-of-equilibrium dynamics can be computed in the HCB limit. We propose to look at the expansion [13, 14, 17, 55] of the cloud when the trap is released to probe the BG phase and the existence of a critical point  $V_2^c = 4$ . Actually, because the trapped ground-state differs from the non-trapped state, what is probed is whether the hamiltonian governing the dynamics induces a localization or not. Expansion is a particularly interesting experiment as, without confinement, the hamiltonian does equal the one of the non-trapped system. Indeed, for a non-trapped system, both the MI and the BG are insulators but, for a trapped cloud

in the MI regime, releasing the trap induces a spreading of the cloud which typical time-scale and features have been widely studied [55]. We show that adding a disordered potential prevents the cloud from expanding in Fig. 17. The system is prepared at time  $t = 0$  in the ground-state of the hamiltonian with the confining potential. At time  $t > 0$ , the trap is removed and the condensate expands on the lattice. For  $V_2 = 0$ , the expansion of the edge of the condensate is roughly linear, with a typical velocity  $2J$  corresponding to the maximum group velocity (see below). For a RBD potential, expansion is inhibited for a strength  $V_2 = 2$ . However, for the bichromatic set-up, the same potential strength does not prevent the condensate from expanding. Still,  $V_2 = 6$  induces a localization of the condensate similar to the one observed for the RBD potential. The important result is thus that the existence

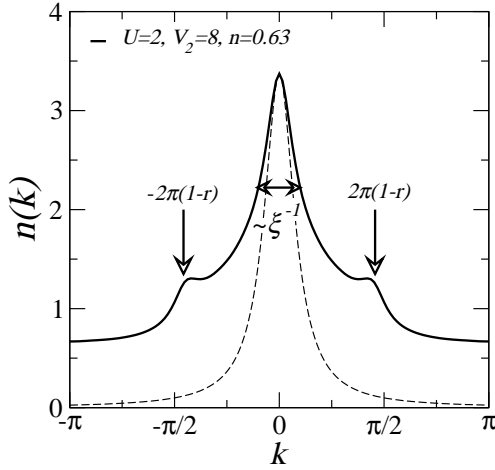


FIG. 16: Typical  $n(k)$  in the Bose-glass phase of Fig. 10 in a system without a trap. Satellites peak at wave vector  $2\pi(1-r)$  are visible if the disorder is not too strong. The middle peak width typically gives the inverse correlation length (a Lorentzian with width  $\xi$  computed from Eq. (12) is given for qualitative comparison with dashed lines).

of a critical value  $V_2^c = 4$  for the localization could be probed experimentally with this technique.

Following Ref. 21, a more precise description of the expansion can be carried out by looking at the one-particle effective dispersion  $\varepsilon(k)$  for HCB. Without translational symmetry, wave vectors  $k$  are not a good quantum number but looking at the Fourier transform of the one-particle wave functions  $\psi_k \sim \sum_j e^{ikj} \psi_j$  and plotting  $|\psi_k|^2$  as a function of the pseudo-momentum  $k$  provides an effective dispersion. The features of the expansion depend mainly on two properties. First, the group velocities  $v_g(k) = \partial\varepsilon(k)/\partial k$  derived from the effective dispersion relation convey the typical maximal speed at which expansion evolves. Second, the expansion also strongly depends on the initial occupation numbers  $n_\varepsilon(t=0)$  of the eigenstates of the hamiltonian without the trap. This occupation is plotted together with the dispersion relation as a function of the “single-particle energy”  $\varepsilon$  in Fig. 18 corresponding to the expansion observed in Fig. 17. For  $V_2 = 2$  for which there is no localization, the effective relation dispersion displays gaps as we have seen from section II and well-defined bands with a shorter periodicity coming from the band folding induced by the potential (see Sec. II). Compared with the simple cosine dispersion of a non-disordered system, several shifted bands (hardly visible) exist due to scattering with the potential. One can convince oneself that opening gaps always lowers the maximum possible group velocity. Thus, compared to a system with no disorder, the expansion for the bichromatic potential below  $V_2 = 4$  will be always slower if the  $\varepsilon = 0$  state (associated with the maximum group velocity  $2J$ ) is occupied for the initial state without disorder. This explains the qualitative features of the situations for which the condensate expands in Fig. 17. Furthermore, the structure of the expansion is richer as inhomogeneity of the condensate is observed during the expansion. These two different speeds might stem from populating bands with different maximum

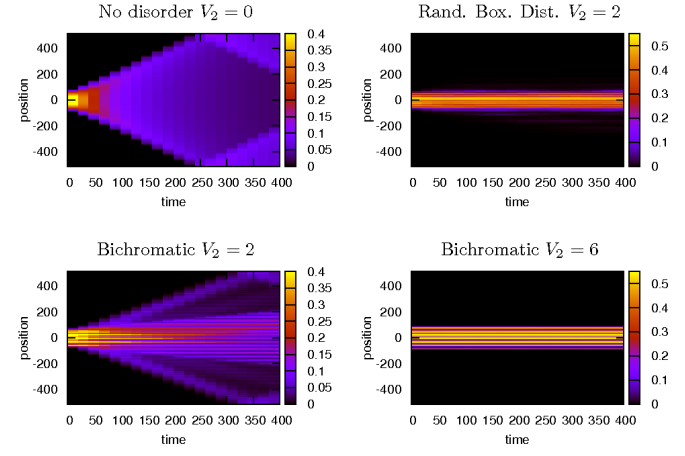


FIG. 17: (Color online) *Expansion of HCB condensates.* At  $t = 0$ , the system is in the ground-state of the hamiltonian with the trap plus “disorder” potentials using a fixed chemical potential  $\mu = -1.5$  and a trap frequency  $\omega = 0.03$ . At  $t > 0$ , the trap confinement is switched off abruptly. Figures shows the evolution of the local density  $n$  as a function of time and position. Expansion is observed for systems with  $V_2 = 0$  (without disorder) and  $V_2 = 2$  but not for a random potential and a bichromatic potential with  $V_2 = 6 > V_2^c$ . Reflexions on the boundaries of the box in which the condensate expands can be seen when expansion is present.

group velocities. For  $V_2 = 6$ , no bands can be distinguished as the signal does not show well-defined pseudo-momentum. The RBD potential displays a dispersion faded by the disorder but which still retains the whole feature of the cosine dispersion without disorder. These two pictures illustrate that the localization mechanism for the bichromatic and a RBD potential is qualitatively different: the first one is rather associated with a band folding mechanism while the second rather corresponds to strongly scattered single-particle states. In this respect, one can view the “weakly superfluid” phase found for commensurate superlattices in Ref. 38 as a precursor of the Bose-glass phase of incommensurate lattices.

## V. CONCLUSION

The Hubbard model with a quasi-periodic potential was shown to display a rich phase diagram including a Bose glass phase (localized with zero one-particle gap excitation), and incommensurate charge-density wave phases in addition to the superfluid and Mott phases. While localization induced by this random-like potential is found, the underlying mechanism differs from the RBD situation: the band folding mechanism known previously for free and hard-core bosons (or fermions) seems to hold for soft-core bosons, leading to a finite critical value of the localization transition  $V_2^c \geq 4$ . The critical values found are high, possibly sufficiently high to allow for an experimental demonstration of a localization-transition in experiments. Static observables for trapped clouds give clear evidences to distinguish between coherent and localized phases, but their ability to sort the BG from the MI phase is less ob-



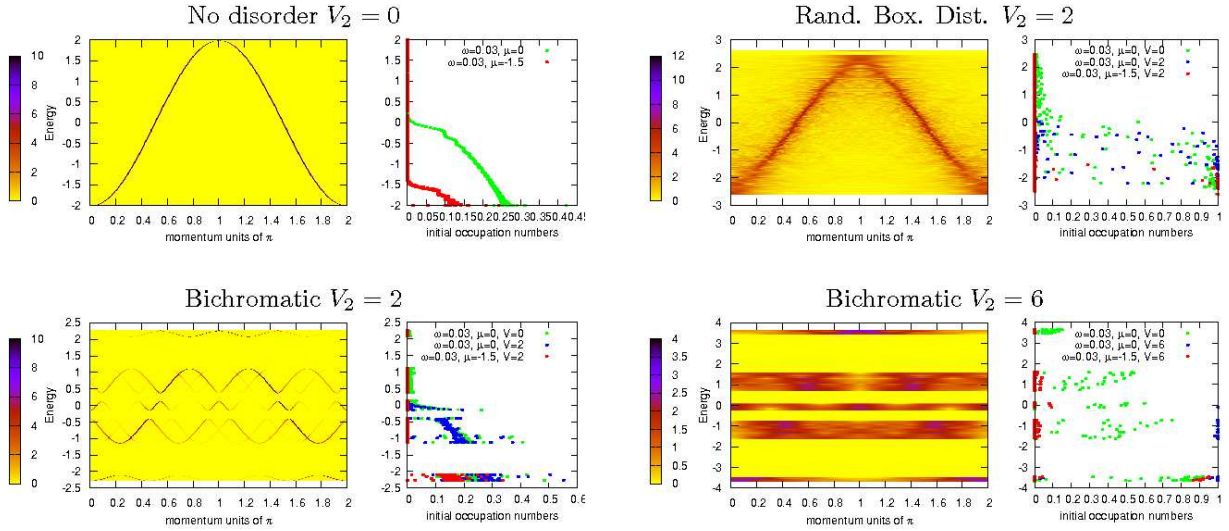


FIG. 18: (Color online) Effective dispersion relations for HCB and initial occupation numbers (see text for details) corresponding to the expansions of Fig. 17.

vious. In this respect, the expansion of the condensate after switching off the confinement is found to provide a simple and rather clear signal to detect the localization transition.

### Acknowledgments

G.R. acknowledges A. Kolezhuk for useful discussions. T.G. thanks M. Inguscio for useful discussions. T.B. thanks the Studienstiftung des deutschen Volkes for financial support. This work was supported in part by the Swiss National Science Foundation under MaNEP and Division II, and by the DFG.

### APPENDIX A: METHOD TO FIT THE BOSONIC GREEN'S FUNCTION ON FINITE SYSTEMS

We use conformal field theory results [44] for a system of length  $L$  with open boundary conditions to fit the bosonic Green's function defined in Eq. (11). In the case of correlations of the type  $\langle e^{i\theta(x)} e^{-i\theta(x')} \rangle$  one has :

$$G(x, x') = A \left[ \frac{\sqrt{d(2x|2L)d(2x'|2L)}}{d(x+x'|2L)d(x-x'|2L)} \right] \frac{1}{2K}, \quad (\text{A1})$$

with  $K$  the Luttinger parameter,  $A$  a constant and  $d$  the conformal length

$$d(x|L) = \frac{L}{\pi} \left| \sin \left( \frac{\pi x}{L} \right) \right|.$$

Because there is no translational invariance, the correlations depend on both  $x$  and  $x'$  so that to perform a fit, one has to average Eq. (A1) over the results with fixed distance  $x' - x$ . Strictly speaking, formula (A1) is valid for  $1 \ll x, x', |x' - x| \ll L$  and we have to remove the corresponding contributions. Practically, fits are rather good up to sizes comparable with  $L$  as one can see in Fig. 19 and improves significantly the determination of  $K$  compared with a simple algebraic fit.

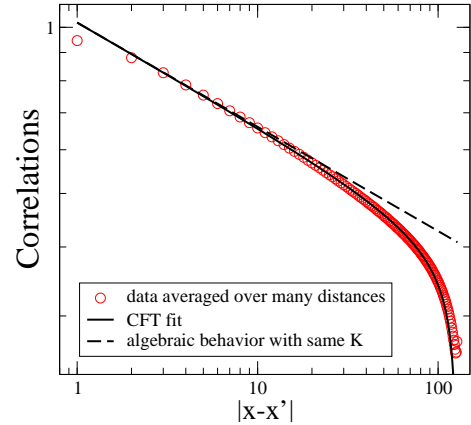


FIG. 19: (Color online) An typical example of fitting the averaged data from DMRG with conformal field theory results to extract the Luttinger exponent  $K$ . System size is  $L = 128$ .

[1] P. W. Anderson, Phys. Rev. **109**, 1492 (1958).

[2] P. A. Lee and T. V. Ramakrishnan, Rev. Mod. Phys. **57**, 287

- (1985).
- [3] E. Abrahams, P. W. Anderson, D. C. Licciardello, and T. V. Ramakrishnan, Phys. Rev. Lett. **42**, 673 (1979).
  - [4] T. Giamarchi and H. J. Schulz, Europhys. Lett. **3**, 1287 (1987).
  - [5] T. Giamarchi and H. J. Schulz, Phys. Rev. B **37**, 325 (1988).
  - [6] M. P. A. Fisher, P. B. Weichman, G. Grinstein, and D. S. Fisher, Phys. Rev. B **40**, 546 (1989).
  - [7] G. G. Batrouni, R. T. Scalettar, and G. T. Zimanyi, Phys. Rev. Lett. **65**, 1765 (1990).
  - [8] R. T. Scalettar, G. G. Batrouni, and G. T. Zimanyi, Phys. Rev. Lett. **66**, 3144 (1991).
  - [9] S. Rapsch, U. Schollwöck, and W. Zwerger, Europhys. Lett. **46**, 559 (1999).
  - [10] N. V. Prokof'ev and B. V. Svistunov, Phys. Rev. Lett. **80**, 4355 (1998).
  - [11] I. Bloch, J. Dalibard, and W. Zwerger, (2007), arXiv:0704.3011.
  - [12] Y. P. Chen *et al.*, (2007), arXiv:0710.5187.
  - [13] D. Clément *et al.*, Phys. Rev. Lett. **95**, 170409 (2005).
  - [14] C. Fort *et al.*, Phys. Rev. Lett. **95**, 170410 (2005).
  - [15] J. E. Lye *et al.*, Phys. Rev. Lett. **95**, 070401 (2005).
  - [16] T. Schulte *et al.*, Phys. Rev. Lett. **95**, 170411 (2005).
  - [17] D. Clément *et al.*, New J. Phys. **8**, 165 (2006).
  - [18] B. Paredes, F. Verstraete, and J. I. Cirac, Phys. Rev. Lett. **95**, 140501 (2005).
  - [19] U. Gavish and Y. Castin, Phys. Rev. Lett. **95**, 020401 (2005).
  - [20] B. Damski, J. Zakrzewski, L. Santos, P. Zoller, and M. Lewenstein, Phys. Rev. Lett. **91**, 080403 (2003).
  - [21] R. B. Diener, G. A. Georgakis, J. Zhong, M. Raizen, and Q. Niu, Phys. Rev. A **64**, 033416 (2001).
  - [22] J. E. Lye *et al.*, Phys. Rev. A **75**, 061603 (2007).
  - [23] L. Fallani, J. E. Lye, V. Guarrera, C. Fort, and M. Inguscio, Phys. Rev. Lett. **98**, 130404 (2007).
  - [24] S. Aubry and G. André, Ann. Israel Phys. Soc **3**, 133 (1980).
  - [25] B. Simon, Adv. Appl. Math **3**, 463 (1982).
  - [26] M. Kohmoto, L. P. Kadanoff, and C. Tang, Phys. Rev. Lett. **50**, 1870 (1983).
  - [27] M. Kohmoto, Phys. Rev. Lett. **51**, 1198 (1983).
  - [28] D. J. Thouless, Phys. Rev. B **28**, 4272 (1983).
  - [29] C. Tang and M. Kohmoto, Phys. Rev. B **34**, 2041 (1986).
  - [30] H. Hiramoto and M. Kohmoto, Int. Jour. of Mod. Phys. B **6**, 281 (1992).
  - [31] F. Piéchon, Phys. Rev. Lett. **76**, 4372 (1996).
  - [32] J. X. Zhong and R. Mosseri, J. Phys.: Cond. Matt. **7**, 8383 (1995).
  - [33] J. Vidal, D. Mouhanna, and T. Giamarchi, Phys. Rev. Lett. **83**, 3908 (1999).
  - [34] J. Vidal, D. Mouhanna, and T. Giamarchi, Phys. Rev. B **65**, 014201 (2001).
  - [35] R. Roth and K. Burnett, Phys. Rev. A **68**, 023604 (2003).
  - [36] P. J. Y. Louis and M. Tsubota, (2006), arXiv:cond-mat/0609195.
  - [37] N. Bar-Gill, R. Pugatch, E. Rowen, N. Katz, and N. Davidson, (2006), arXiv:cond-mat/0603513.
  - [38] V. G. Rousseau *et al.*, Phys. Rev. B **73**, 174516 (2006).
  - [39] P. Buonsante and A. Vezzani, Phys. Rev. A **70**, 033608 (2004).
  - [40] P. Buonsante, V. Penna, and A. Vezzani, Phys. Rev. A **72**, 031602 (2005).
  - [41] T. Roscilde, (2007), arXiv:0712.2741.
  - [42] [http://en.wikipedia.org/wiki/Continued\\_fraction](http://en.wikipedia.org/wiki/Continued_fraction).
  - [43] F. D. M. Haldane, Phys. Rev. Lett. **47**, 1840 (1981).
  - [44] M. A. Cazalilla, J. Phys. B **37**, S1 (2004).
  - [45] T. Giamarchi, *Quantum Physics in one Dimension* International series of monographs on physics Vol. 121 (Oxford University Press, Oxford, UK, 2004).
  - [46] G. I. Dzharapadze and A. A. Nersesyan, JETP Lett. **27**, 334 (1978).
  - [47] V. L. Pokrovsky and A. L. Talapov, Phys. Rev. Lett. **42**, 65 (1979).
  - [48] H. J. Schulz, Phys. Rev. B **22**, 5274 (1980).
  - [49] J. M. Kosterlitz and D. J. D J Thouless, J. Phys. C: Solid State Phys. **6**, 1181 (1973).
  - [50] J. M. Kosterlitz, J. Phys. C: Solid State Phys. **7**, 1046 (1974).
  - [51] V. L. Berezinskii, Sov. Phys. JETP **32**, 493 (1971).
  - [52] T. D. Kühner, S. R. White, and H. Monien, Phys. Rev. B **61**, 12474 (2000).
  - [53] T. Giamarchi, Physica B **230**, 975 (1997).
  - [54] M. Arlego, D. C. Cabra, and M. D. Grynberg, Phys. Rev. B **64**, 134419 (2001).
  - [55] M. Rigol and A. Muramatsu, Mod. Phys. Lett. B **19**, 861 (2005).
  - [56] S. R. White, Phys. Rev. Lett. **69**, 2863 (1992).
  - [57] S. R. White, Phys. Rev. B **48**, 10345 (1993).
  - [58] U. Schollwöck, Rev. Mod. Phys. **77**, 259 (2005).
  - [59] P. Schmitteckert, T. Schulze, C. Schuster, P. Schwab, and U. Eckern, Phys. Rev. Lett. **80**, 560 (1998).
  - [60] K. Hida, Phys. Rev. Lett. **86**, 1331 (2001).
  - [61] C. Schuster, R. A. Römer, and M. Schreiber, Phys. Rev. B **65**, 115114 (2002).
  - [62] I. P. McCulloch, J. Stat. Mech.: Theor. Exp. , P10014 (2007).
  - [63] D. Barache and J. M. Luck, Phys. Rev. B **49**, 15004 (1994).
  - [64] C. Kollath, U. Schollwöck, J. von Delft, and W. Zwerger, Phys. Rev. A **69**, 031601 (2004).